Synthesis strategies to control the Al distribution in zeolites: thermodynamic and kinetic aspects

Juna Bae and Michiel Dusselier [ID] *

The activity and selectivity of acid-catalyzed chemistry is highly dependent on the Brønsted and Lewis acid sites generated by Al substitutions in a zeolite framework with the desired pore architecture. The siting of two Al atoms in close proximity in the framework of high-silica zeolites can also play a decisive role in improving the performance of redox catalysts by producing exchangeable positions for extra-framework multivalent cations. Thus, considerable attention has been devoted to controlling the Al incorporation through direct synthesis approaches and post-synthesis treatments to optimize the performance as (industrial) solid catalysts and to develop new acid- and redox-catalyzed reactions. This Feature Article highlights bottom-up synthetic strategies to fine-tune the Al incorporation in zeolites, interpreted with respect to thermodynamic and kinetic aspects. They include (i) variation in extra-framework components in zeolite synthesis, (ii) isomorphous substitution of other heteroatoms in the zeolite framework, and (iii) control over the (alumino)silicate network in the initial synthesis mixture *via in situ* and *ex situ* methods. Most synthetic approaches introduced here tentatively showed that the energy barriers associated with Al incorporation in zeolites can be variable during zeolite crystallization processes, occurring in complex media with multiple chemical interactions. Although the generic interpretation of each strategy and underlying crystallization mechanism remains largely unknown (and often limited to a specific framework), this review will provide guidance on more efficient methods to prepare fine-tuned zeolites with desired chemical properties.

Center for Sustainable Catalysis and Engineering (CSCE), KU Leuven, Celestijnenlaan 200F, 3001 Leuven, Belgium. E-mail: michiel.dusselier@kuleuven.be

Juna Bae received her PhD in Chemical Engineering from POSTECH (South Korea) in 2020 under the guidance of Prof. Suk Bong Hong, studying the synthesis of zeolites with novel framework structures and/or compositions using simple organic structure-directing agents. In 2020–2021, she stayed with the same group and focused her reseach on the effect of fluoride concentration in the initial synthesis mixture on zeolite crystallization. Since 2021, she has been a postdoctoral researcher in the Dusselier group, working on the synthesis of small- and medium-pore zeolites with controlled acid sites.

Juna Bae

Prof. Michiel Dusselier obtained his PhD (Bioscience Engineering Catalytic Technology, 2013) at KU Leuven, Belgium, working on catalysis for bioplastics synthesis. In 2014–2015, he did postdoctoral work at Caltech, USA, looking into AEI and GME zeolite syntheses. He is now an associate professor at KU Leuven and co-founded the new Center for Sustainable Catalysis and Engineering in 2019. He is focusing on zeolite synthesis methods including reactor design (subject of an ERC Starting Grant), degradable plastics and heterogeneous catalysis (CO_2 activation). He has authored ca. 70 peer-reviewed papers and 12 patents, of which one transferred to industry. In 2022, he received the Young Researcher Award of the International Zeolite Association.

Michiel Dusselier

Introduction

Zeolites are crystalline, microporous materials constructed by corner-sharing SiO_4 and AlO_4^- tetrahedra and are used commercially as adsorbents, ion exchangers, and catalysts.[1–3] Their performance is related to the density, strength, and location of intrazeolitic active sites, as well as the size, shape, and dimensionality of the pore systems containing regular channels and cavities. Brønsted acid sites in zeolites, acting as the active site in acid-catalyzed reactions, are generally created when protons compensate for the negative framework charges induced by incorporating Al^{3+} into a silica framework. It is thus not difficult to see that the position and relative concentration of Al atoms in the tetrahedral sites (T-sites) of the framework can alter the location and properties of acid sites in zeolites. Furthermore, the distribution of proximal Al sites (*i.e.*, Al–O–(Si–O)$_x$–Al, x = 1 or 2) can generate exchangeable sites to stabilize multivalent extra-framework species (*e.g.*, Cu, Co, Fe). Apart from its effect on the formation of active sites for redox catalysts,[4–11] the proximity of Al sites in the framework has been demonstrated to influence the selectivity in acid-catalyzed reactions, giving very different results from materials with nearly equal amounts of framework Al content.[12–15]

In the aluminosilicate zeolites with relatively high framework Al contents (Si/Al < 5), most Al atoms are separated by single Si atoms (*i.e.*, Al–O–Si–O–Al sequence). In contrast, various Al arrangements can be distributed in Si-rich zeolites with the exception of the formation of Al–O–Al linkages according to Löwenstein's rule.[16] To understand structure-activity relations and ultimately design more finely tuned catalysts, it is important to evaluate the position and distribution of Al atoms in a given zeolite framework. For quantitatively probing the location and proximity of Al atoms, various analysis methods, such as FT-IR, solid-state NMR, X-ray based techniques (*i.e.*, 3D scanning transmission X-ray microscopy, X-ray diffraction, X-ray standing waves, X-ray absorption spectroscopy, X-ray emission spectroscopy, *etc.*), and titration by divalent metal cations, have been applied, along with theoretical calculations.[9,17–31] In particular, the Co^{2+} titration method combined with UV-visible spectroscopy has widely been adopted to indirectly analyze the number of paired (or proximate) *vs.* isolated Al atoms (*i.e.*, Al–O–(Si–O)$_x$–Al, x = 1, 2 *vs.* ≥3, respectively). However, due to limitations such as very similar scattering factors of Si and Al for X-rays and structural degradation caused by thermal or synthesis treatments, obtaining direct evidence of the exact Al siting remains one of the most challenging issues in structural zeolite science. Furthermore, the dynamic nature of active sites at operando conditions makes it difficult to directly link the structure-activity relationship.[32]

First-generation zeolites synthesized without any organic additives (before the 1960s) typically have a Si/Al ratio of less than 5. The use of alkylamines and alkylammonium ions commonly acting as organic structure-directing agents (SDAs) has long been recognized as one of the best-known strategies for controlling the Al incorporation in the resulting zeolites.[33,34] Indeed, many synthetic strategies are based on the introduction of a broad spectrum of organic SDAs, such as charge density mismatch approach, supramolecular self-assembly, and alkali metal-crown ether complexes.[35–40] These have led to the expansion of the compositional range of crystalline microporous materials. In addition to the direct synthesis approaches through changes in the chemical/physical environment, the possibility of engineering the Al distribution through post-synthesis modifications such as dealumination (*e.g.*, the ultrastable Y series), alumination, or consecutive demetallation and alumination has also been explored heavily.[41–43]

There have been several review articles on the analysis and regulation of active sites in zeolites and the effect of modified sites on the catalytic performance.[31,41,42,44–46] In this Feature Article we focus on key aspects of direct bottom-up synthetic strategies with the aim of addressing the impact of thermodynamic *vs.* kinetic contributions on the Al incorporation in zeolites. We divide them with respect to the creation of new chemical environments in the synthesis mixture based on simple compositional variations of (i) extra-framework components and (ii) heteroatoms for isomorphous substitution in zeolite frameworks and (iii) control of the (alumino)silicate network in the initial synthesis mixtures with same (or similar) oxide composition. These three classifications are roughly divided as they can be seen as subject to more thermodynamic (i and ii) or more kinetic control (iii), respectively. We also discuss how these factors can support the rational design of zeolites with desired chemical properties.

Effect of extra-framework components in zeolite synthesis

Extra-framework components in a synthesis are defined as species that do not end up part of the tetrahedral lattice of a zeolite; *i.e.*, SDAs and mineralizing agents.

Cooperative structure-directing effect: I. dual organic SDAs

The introduction of organic SDAs in zeolite synthesis offered a major breakthrough in the discovery of new zeolites. The positively charged SDAs can interact with negatively charged oxygen of framework AlO_4^- units. They usually end up entrapped inside certain void spaces of resulting zeolite, but the geometric correspondence between the porous channel/cage and organic SDA is generally not high. However, it is well established that the framework topology and/or composition of the zeolite product can be strongly influenced by the properties of the organic SDAs employed, such as size, shape, rigidity/flexibility, hydrophobicity/hydrophilicity, and charge distribution.[37,47–50] Based on this fact, much effort has been devoted to understanding the cooperative effects of multiple SDAs on the regulation of the spatial distribution of Al atoms in the zeolite framework.

FER. Pinar and co-workers demonstrated, in a pioneering effort, that the location of Al atoms over the four crystallographically distinct T-sites in the ferrierite (FER) topology can be altered depending on the specific combination of

tetramethylammonium (TMA$^+$) ions with other organic molecules such as pyrrolidine (PYR) and benzylmethylpyrrolidinium (BMP$^+$) ions. FER-PYR, FER-PYR-TMA, and FER-BMP-TMA with similar Si/Al $\sim$ 15 were synthesized from PYR alone and PYR-TMA and BMP-TMA dual-SDA systems. Their ^{27}Al MAS NMR spectra could not yield quantitative conclusions, but clearly exhibited differences in the relative intensity of the two tetrahedral ^{27}Al resonances at 56 and 53 ppm.[51]

Rietveld refinement of the structure of FER-PYR and FER-PYR-TMA with the unit cell compositions of |PYR$_{4-x}$TMA$_x$H$_2$|-[Si$_{34}$Al$_2$O$_{72}$], x = 0 and 0.4, respectively, revealed that TMA$^+$ ions exist only in the *fer* ([5^{8}6^{6}8^2]) cavity, whereas PYR species are located within both the *fer* cavity and the main 10-ring channel.[24] PYR species (likely protonated) present in both samples were analyzed to interact more strongly with framework oxygen atoms in *fer* cavities than those in the main 10-ring channels. Their interactions are also stronger than those with TMA$^+$ ions, suggesting the strong effect of PYR on the distribution of Al atoms in FER. Especially, the partial replacement of PYR with TMA$^+$ within the *fer* cavity (*i.e.*, FER-PYR-TMA) reduces the occupancy of Al atoms at T$_3$ site (in the inner part of the *fer* cavity), whereas Al atoms are preferentially sited at T$_1$ site (in the 8-ring connecting the main 10-ring channel and the cavity) (Fig. 1a). The Rietveld refinement results are consistent with the experimentally observed proton accessibility of pyridine,[52] as well as the computational results.[53] As a consequence of the preferential location of Al atoms in the 10-ring channels, the catalytic activity of FER-PYR-TMA in the isomerization of *m*-xylene and 1-butane reactions increased.[52,54] Under almost identical synthesis conditions, on the other hand, Davis and co-workers showed that the synthesis of FER (Si/Al $\sim$ 17) using hexamethyleneimine (HMI), larger size than PYR, in combination with TMA$^+$ ions as co-SDA increased the amount of acid sites located in the 10-ring channels.[55]

FAU. Dusselier and co-workers applied the cooperative strategy of dual organic SDAs to regulate the Al content in FAU zeolites.[56] The cooperative structure direction between 1,4,7,10,13-pentaoxacyclopentadecane (15-crown-5, CE) and (2-hydroxyethyl)trimethylammonium (choline, Ch$^+$) was adopted in the presence of Na$^+$. Both organics have been reported to direct FAU zeolites with Si/Al ratios below 5.[57–59] When CE is used as the sole organic SDA, its intrazeolitic location is known to be in the supercage of FAU zeolite with Si/Al ratio of 4.5 by forming a cationic complex with Na$^+$ (*i.e.*, Na$^+$-15-crown-5). In the case of using Ch$^+$ for FAU (Si/Al = 2.0) a small fraction (8%) of Ch$^+$ ions can be located in *sod* cages as a *trans* conformer, but most (81%) are present in supercages as a *gauche* conformer.

Based on their intrazeolitic locations, optimum synthesis conditions were investigated in order to place a higher content of *trans* Ch$^+$ within *sod* cages, while Na$^+$-15-crown-5 complex and *gauche* Ch$^+$ were occupied in the supercage (Fig. 1b). The use of CE as the cooperative organic SDA under optimized synthetic conditions was shown to promote the fraction of *trans* Ch$^+$ (51% of total Ch$^+$) which is mainly in the *sod* cages, whereas the total number of Ch$^+$ ions per unit cell did not change. This is suggested to lead to competition between *trans* Ch$^+$ and Na$^+$ for *sod* (and other) cages, which resulted in high-silica (Si/Al = 6) FAU zeolite with low Na$^+$ content. This result also suggests that the control of the intrazeolitic location of specific organic molecule *via* the cooperative strategy of multiple organic SDAs might influence the spatial disribution of Al atoms. Although further investigation into the Al distribution
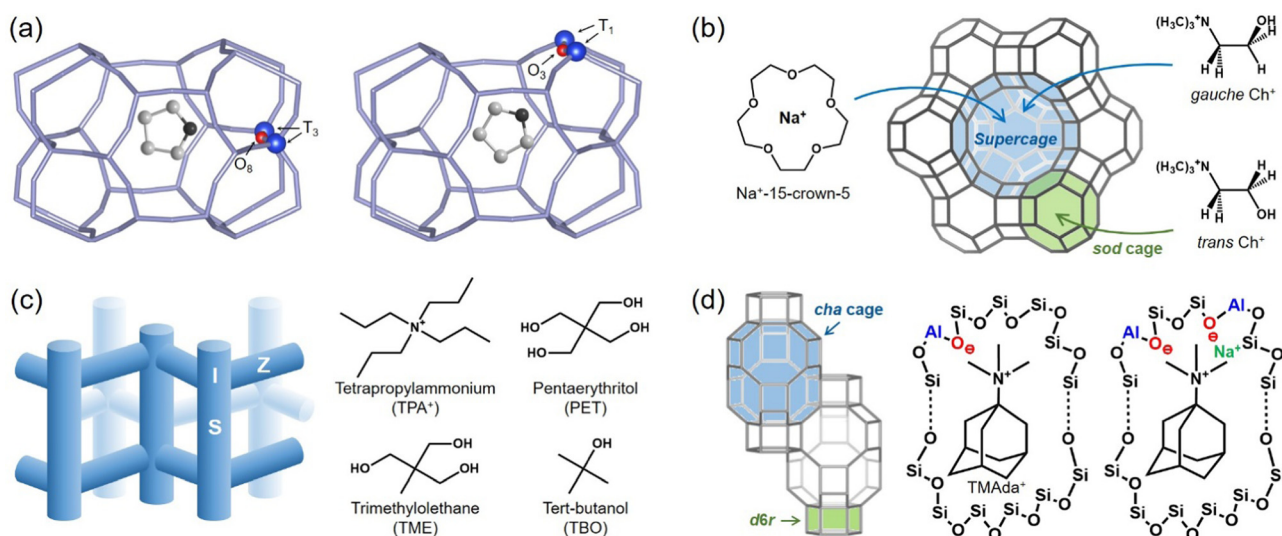
Fig. 1 Cooperative effects of multiple SDAs. (a) The *fer* ([5^{8}6^{6}8^2]) cavity of the FER structure containing pyrrolidine (PYR) synthesized from PYR alone (left) and PYR-TMA dual-SDA system (right), where the TMA$^+$ is not shown but is presumed to reside in the other *fer* cavity. Adapted from ref. 24. (b) Scheme of the cooperative strategy of Na$^+$-15-crown-5 complex and *gauche* and *trans* Ch$^+$ conformers for high-silica (Si/Al = 6) FAU zeolite synthesis. Adapted from ref. 56. (c) Scheme of the channel system of ZSM-5 (MFI) containing straight (S) 10-ring channels intersected (I) by sinusoidal (Z) 10-ring channels. TPA$^+$ and branched alcohols (*e.g.*, PET, TME, TBO) are preferentially occupied in the channel intersections (I). (d) The CHA structure with two composite building units, *cha* cage and *d6r*, and scheme of the Al arrangement during CHA crystallization in the presence of TMAda$^+$ alone (left) and in combination with Na$^+$ ions (right). Adapted from ref. 67.

of FAU zeolite synthesized in the CE-Ch$^+$ dual-SDA system needs to be performed, its proton form showed improved catalytic performance in the pyrolysis of low-density polyethylene, compared to the proton form of commercial USY zeolite (H-CBV712) with almost the same Al content (Si/Al = 6), but less Brønsted and Lewis acid sites estimated by pyridine-IR.

Recent studies on the relationship between (controlled) accessibility of the active sites in the *sod* cage and catalytic performance also showed that changes in the content and distribution of Al atoms, especially in *sod* cages, could be responsible for the exceptional catalytic activity.[60,61] On the other hand, Wakihara and co-workers showed the synthesis of high-silica (Si/Al = 4.2 or 6) FAU zeolites using *N,N*-dimethyl-3,5-dimethylpiperidinium or tetrapropylammonium (TPA$^+$), respectively, as the sole organic SDA, and found higher fraction of Q^4(1Al) species than those from previously reported FAU zeolites.[62] This implies that these two organics could be promising candidates for cooperative organic strategies for high-silica FAU zeolites with unique Al distributions.

Cooperative structure-directing effect: II. inorganic and organic SDAs

MFI. Yokoi and co-workers reported a strategy to control the location of Al atoms in ZSM-5 (MFI, Si/Al $\sim$ 50) using various organic molecules (*e.g.*, TPA$^+$, dipropylamine, cyclohexylamine, HMI) in the presence or absence of Na$^+$ cations.[63] The concentration of acid sites and the strength of Brønsted acidity in the proton form of each zeolite were not significantly affected by the type of the organic molecules or the presence of Na$^+$ cations. However, the distribution of acid sites estimated using the constraint index (CI) was highly dependent on the presence of Na$^+$ cations in synthesis mixtures. The CI value was calculated as the ratio of the first-order rate constant in the cracking reactions of *n*-hexane and 3-methylpentane. This showed that higher amount of acid sites located in larger spaces (*i.e.*, in the channel intersections (I) instead of straight (S) and sinusoidal (Z) channels (Fig. 1c)) correlated with lower CI values.

ZSM-5 obtained using only TPA$^+$ ions was calculated to have the lowest Cl value (1.7), indicating that the Al atoms prefer to be located at the channel intersections. When Na$^+$ cations were added to the TPA$^+$-containing synthesis mixture, however, this value increased to 5.2. This can be explained by the change in the location of some Al atoms from the intersections to narrow straight and/or sinusoidal 10-ring channels. Interestingly, there is a non-negligible dissimilarity between the number of framework Al atoms and the sum of TPA$^+$ and Na$^+$ ions, *i.e.*, Si/Al = 52, TPA$^+$/Al = 2.3 and (TPA$^+$ + Na$^+$)/Al = 3.1. This indicates that some of the TPA$^+$ ions predominantly occluded at the four intersections may serve as pore-filling species, presumably interacting with framework defects, rather than as charge-compensating cations.

Similarly, the distribution of Al atoms in ZSM-5 with Si/Al = 19–28 was controlled using various alcohols as non-charged, pore-filling agents together with Na$^+$ ions.[64–66] For example, branched alcohols (*e.g.*, pentaerythritol (PET), trimethylolethane (TME), *tert*-butanol (TBO)) have a molecular structure similar to TPA$^+$ ion (Fig. 1c). These non-charged molecules were preferentially occupied in the channel intersections, making Na$^+$ ions mainly located in straight and/or sinusoidal channels. On the other hand, ZSM-5 synthesized with straight-chain alcohols (*e.g.*, 1,3-propanediol, 1,6-hexanediol, diethylene glycol, triethylene glycol, glycerol) showed different Al distribution according to the length of alcohol molecules and content introduced. This is because they can be positioned at both the channels and intersections.

CHA. The cooperative (or competitive) effects of inorganic and organic SDA combinations on the arrangement of Al was observed in the crystallization of CHA zeolites. Gounder and co-workers crystallized a series of CHA (Si/Al $\sim$ 14–18 and other values) zeolites by comparing the effects of the type and concentration of alkali cations in the presence of *N,N,N*-trimethyl-1-adamantylammonium (TMAda$^+$) ions.[67,68] When TMAda$^+$ was used alone or in combination with K$^+$ ions, no (or lower amounts of) 6MR paired (or 'proximate') Al sites quantified by Co^{2+} titration were observed. However, the partial replacement of TMAda$^+$ with Na$^+$ in the synthesis mixture resulted in the formation of proximate Al atoms (Co/Al = 0.08) (Table 1 entries 7, 8, 10 and 11 and Fig. 1d and 2). They found that the Na$^+$/TMAda$^+$ ratio in the synthesis mixture is an important factor governing the proportion of proximal Al atoms (paired sites) in a given zeolite (Fig. 2), and the pairing increased linearly with the content of occluded Na$^+$ in the crystalline products. The increase in proximal protons in CHA zeolites with similar composition (Si/Al $\sim$ 14–18) enhanced turnover rates for methanol dehydration to dimethyl ether (per H$^+$, 415 K) by stabilizing surface methoxy species involved in the dissociative dehydration pathway.[14]

A combination of elemental analysis and theoretical calculation revealed that each *cha* cage in as-made CHA zeolites obtained from the TMAda$^+$–Na$^+$-containing synthesis media was calculated to contain one TMAda$^+$ ion on average, regardless of the amount of co-occluded Na$^+$ ions in the 6MR (0–0.3 Na$^+$ per cage (or double 6-ring (*d6r*) unit).[67] This may promote the formation of particular framework Al arrangements in 6MR. In contrast, the use of K$^+$ instead of Na$^+$ halved the occupancy of TMAda$^+$ in *cha* cages while increasing the content of K$^+$ ions (0–1.2 per cage) by competitive positioning within *cha* cages (*e.g.*, 8MR).[68] The effect of various alkali metal cations (*e.g.*, Li$^+$, Na$^+$, K$^+$, Cs$^+$) in combination with TMAda$^+$ ions on the proximity of Al atoms was also confirmed by Fan and co-workers in CHA zeolites with Si/Al $\sim$ 10.[69] The formation of paired Al atoms was most promoted by Li$^+$ ions, and decreased as the radii of alkali metal ions increased (Table 1 entries 1–4).

Recently, Xiao and co-workers examined the effect of altered formation pathways on the location of Al atoms in CHA zeolites (Si/Al $\sim$ 10) depending on the type of organic SDA employed (*e.g.*, TMAda$^+$, *N,N*-dimethylcyclohexylammonium (DMCHA$^+$)).[70] Based on the 2D ^{1}H DQ-SQ NMR, Raman, and FT-IR spectroscopies, the crystallization mechanisms for CHA zeolite crystals were suggested. In the TMAda$^+$–Na$^+$ system, the nucleation is proposed to begin with the formation of 8MRs through strong electrostatic interactions between TMAda$^+$ and the defect sites

Table 1 Representative synthesis conditions for a series of high-silica SSZ-13 (CHA) zeolites and their Si/Al and Co/Al ratios

| Entry | Sources | R[a] | Synthesis mixtures composition relative to Si | | | | Si/Al$_{prod.}$ | Co/Al | Ref. |
			ROH	MOH	Al	H$_2$O			
1	Silica sol, Al$_2$(SO$_4$)$_3$	TMAda$^+$	0.40	0.3Li$^+$	0.100	88	9.5	0.22	69
2	Silica sol, Al$_2$(SO$_4$)$_3$	TMAda$^+$	0.40	0.3Na$^+$	0.100	88	10.3	0.14	69
3	Silica sol, Al$_2$(SO$_4$)$_3$	TMAda$^+$	0.40	0.3K$^+$	0.100	88	10.2	0.08	69
4	Silica sol, Al$_2$(SO$_4$)$_3$	TMAda$^+$	0.40	0.3Cs$^+$	0.100	88	11.0	0.05	69
5	Ludox AS-40, NaAlO$_2$	TMAda$^+$	0.12	0.36Na$^+$	0.064	22	9.6	0.24	70
6	Ludox AS-40, NaAlO$_2$	DMCHA$^+$	0.12 (Br$^-$ form)	0.36Na$^+$	0.070	—[b]	10.2	0.42	70
7	Ludox HS-40, Al(OH)$_3$	TMAda$^+$	0.50	—	0.067	44	14.5	0.00	67
8	Ludox HS-40, Al(OH)$_3$	TMAda$^+$	0.25	0.25Na$^+$	0.067	44	14.8	0.08	67
9	Ludox HS-40, Al(O-i-Pr)$_3$	TMAda$^+$	0.25	0.25Na$^+$	0.067	44	14–18	0.22	14
10	Ludox HS-40, Al(OH)$_3$	TMAda$^+$	0.25	0.25K$^+$	0.067	44	15.0	0.05	68
11[c]	Ludox HS-40, Al(OH)$_3$	TMAda$^+$	0.024–0.125	0.375–0.467K$^+$	0.067	44	10–14	<0.01	68
12	CBV780, (FAU, Si/Al = 40)	TMAda$^+$	0.35	—	0.025	12.5	∼35	0.31	11
13	CBV780, (FAU, Si/Al = 40)	TMAda$^+$	0.175	0.175Na$^+$	0.025	12.5	∼35	0.25	117
14	CBV8014, (MFI, Si/Al = 40)	TMAda$^+$	0.35	—	0.025	12.5	26.2	0.06	11
15	Ludox HS-40, Al(OH)$_3$	TMAda$^+$	0.35	—	0.025	12.5	28.0	0.00	11

[a] R is organic SDA, TMAda$^+$ = N,N,N-trimethyl-1-adamantylammonium, DMCHA$^+$ = N,N-dimethylcyclohexylammonium. [b] Synthesized from solvent-free route. [c] The total cationic charge in the synthesis mixture was fixed at (TMAda$^+$ + K$^+$)/Si = 0.50.
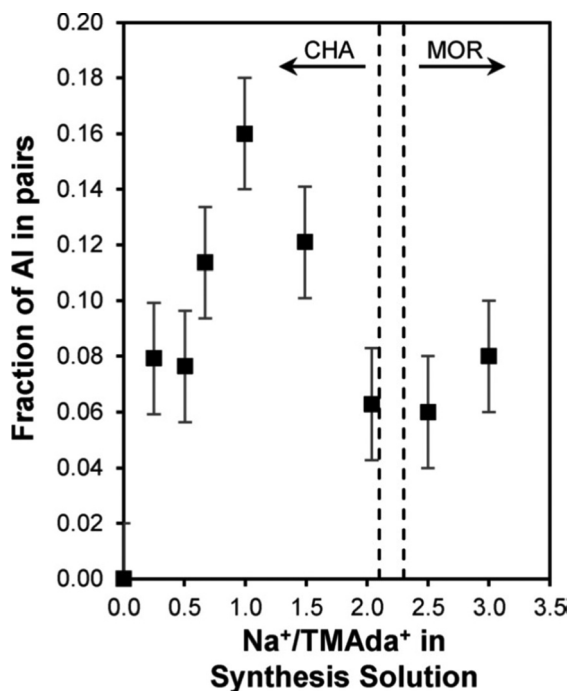
Fig. 2 The fraction of paired Al in a series of SSZ-13 zeolites (CHA, Si/Al ∼ 14–18) synthesized as a function of the Na$^+$/TMAda$^+$ ratio in the synthesis mixtures containing fixed total cationic charge at (TMAda$^+$ + Na$^+$)/Si = 0.50. A mixed CHA/MOR phase is observed in the region between dashed lines. Reproduced with permission from ref. 67. Copyright 2016 American Chemical Society.

($i.e.$, SiO$^-$···HO–Si). In the DMCHA$^+$–Na$^+$ system, however, DMCHA$^+$ ions interacting strongly with the negative Si–O–Al structural units preferentially induce the $d6r$ units over cha cages, leading to much more paired Al atoms (Co/Al = 0.42 $vs.$ 0.24) (Table 1 entries 5 and 6). On the other hand, a recent theoretical investigation into the relationship between the spatial charge distribution of organic SDA and the distribution of Al atoms in CHA structure suggested that more charge-biased organic SDAs in the presence of Na$^+$ ions favor the formation of paired Al sites in $d6r$ units.[50]

Overall, this section demonstrates that the control of Al distribution is possible via the cooperative structure direction of multiple SDAs. This could be realized by (i) the proper selection of size, shape, and charge distribution of SDAs and (ii) the competition among multiple SDAs to interact with framework negative AlO$_4^-$ charges instead of defect sites. Although kinetic factors may compete (or overlap) with energetic interactions, the geometric- and/or electrostatic-based thermodynamic properties of multiple SDAs can be used to predict and design the Al distribution in zeolite frameworks.

Fluoride anions as an inorganic synthesis parameter

The use of fluoride anions as a mineralizing agent in zeolite synthesis was first introduced by Flanigen and Patton in 1978 to crystallize pure-silica ZSM-5 at near-neutral pH ($vs.$ typically pH > 11).[71] Since then, the fluoride route has been successfully applied in the discovery of numerous zeolites and related materials with new framework topologies and/or compositions.[37,72,73] It has generally been realized with equimolar amounts of F$^-$ and organic SDA under highly concentrated conditions, especially when properly combined with the ability of certain organic SDAs and/or other heteroatoms ($e.g.$, Ge). In many cases, it has been shown that F$^-$ anions are encapsulated within small cages like double-4-ring ($d4r$) units in assynthesized zeolites. This indicates that F$^-$ anions could act as a factor determining the phase selectivity of the crystallization, as well as a counter-anion balancing the positive charge introduced by the organic SDAs. In addition, F$^-$ anions entrapped within the crystallized products can compete with the introduction of heteroatoms into silica frameworks.

In this regard, Hong and co-workers investigated the concentration effect of F^- as an inorganic synthesis parameter on the zeolite product in the synthesis mixture with a certain amount of lattice charge. Recently, they were able to discover four novel (alumino)silicate zeolites (i.e., PST-21 (PWO), PST-22 (PWW), PST-24, and PST-30 (PTY)) in the presence of different mono- and diquaternary diazolium-based cations as organic SDAs (OSDAs) under excess fluoride conditions (HF/OSDA^{n+} ≥ 2n, where n is 1 or 2).[40,74–76] The excess fluoride approach (HF/OSDA = 2) also allowed them to synthesize a high-silica (Si/Al = 14) version of zeolite ERS-7 (ESV) using choline (Ch$^+$) ions.[77] Considering the unit cell composition and multinuclear MAS NMR results, they suggested that some F^- anions paired with Ch$^+$ located within large 17-hedral ($[4^6 5^4 6^5 8^2]$) picnic-basket-shaped cages make the resulting zeolite more siliceous.

The same research group also found that F^- concentration in the synthesis mixture in the presence of N,N-dimethyl-piperidinium ions as an organic SDA can influence the framework Al distribution over the two distinct T-sites in levyne (LEV) structure (Fig. 3a).[78] Levyne crystallized over a wide range (0.5–2.0) of HF/OSDA ratios in the synthesis mixture with Si/Al = 10. However, F^- concentration has little effect on the degree of Al substitution (Si/Al ∼ 11.0), as well as the F^- content (negligible amount confirmed by ^{19}F MAS NMR spectroscopy) within their as-synthesized form. Further increase in F^- concentration in the synthesis mixture produced a mixture of ESV and NON at HF/OSDA = 3.0 and a dense phase at HF/OSDA = 4.0. As the HF/OSDA ratio in the synthesis mixture was increased from 0.5 to 2.0, the relative intensity ratio of the two deconvoluted tetrahedral ^{27}Al resonances at 57 and 53 ppm decreased from 0.53 to 0.36 (Fig. 3b). The high- and low-field ^{27}Al NMR resonances could be assigned to Al atoms in the T_1 and T_2 sites with multiplicities of 36:18 of the LEV framework by calculating average Al–O–Si angles using the equation of Jacobsen et al.[79] Each value is also significantly lower than the ideal ratio (2.0) for the statistical distribution of Al atoms over the LEV structure. This suggests that the F^- anions in the synthesis mixture may act as a factor to selectively distribute Al atoms to specific T-sites during the nucleation and crystal growth processes.

A similar approach was considered by Liu and co-workers.[80] A series of high-silica (Si/Al ∼ 280) beta (*BEA) zeolites were synthesized by changing the HF/SiO$_2$ ratio in the synthesis mixture. Different Al distributions in *BEA framework were observed by ^{27}Al MAS and ^{27}Al MQ MAS NMR spectroscopy. The authors analyzed the Al T-site distribution based on the DFT calculations reported by Lercher and co-workers.[28] When increasing the HF/SiO$_2$ ratio from 0.45 to 0.65, the relative content of Al atoms located at T_9 site gradually decreased, while the content at T_8 sites correspondingly increased. However, it is not easy to deconvolute the spectra and assign them to the Al atoms in specific T-sites due to the multiple overlapped resonances characteristic of this disordered material with high number (9) of distinct framework positions.

These synthetic efforts indicate that the incorporation of Al atoms in zeolites can be altered by properly changing the F^- concentration in the synthesis mixture. However, the exact role of F^- as an inorganic synthesis variable in determining the Al incorporation, especially its interaction with other synthetic parameters (e.g., Al, organic/inorganic cationic SDAs) and how this contributes to the distribution and structure of (alumino)-silicate species during the nucleation stage, remains to be elucidated.

Effect of isomorphous substitution in zeolite frameworks

The isomorphous substitution of Al and/or Si (and P) by other heteroatoms (e.g., B, Ga, Ge, Sn, Zn, etc.) in the zeolite frameworks during the crystallization process is known as an efficient way to tune the physicochemical and catalytic properties for specified applications, as well as to synthesize novel framework topologies.[41] In several papers, the spatial distribution of heteroatoms other than Si has proved to be non-random, reflecting the preference of a given heteroatom for positioning at particular T-sites. In addition, this implies that the incorporation of a second tri- or tetravalent heteroatom can be used to optimize the distribution and content of Al atoms in zeolite framework.

B,Al-MWW

Wang and co-workers regulated the Al distribution in MCM-22 (MWW) zeolite by introducing boron (B) as a second trivalent heteroatom.[81] According to DFT calculations, the Al incorporation over the eight distinct T-sites in MWW is preferred in the order of $(T_4, T_2) > (T_6, T_8, T_3) > (T_7, T_5, T_1)$,[82] whereas in the case of B, the order is $(T_2, T_1) > (T_3, T_8, T_5) > (T_7, T_6) > T_4$ (Fig. 4). This suggests that the competitive siting between Al and B may occur thermodynamically at T_2, T_8, and T_3 sites rather than T_4 and T_6 sites. B- and Al-containing MCM-22 zeolites with different B contents but almost the same Al

Fig. 3 (a) The LEV structure with two crystallographically distinct T-sites. Red and blue circles represent T_1 and T_2 sites, respectively. O atoms omitted for clarity. (b) ^{27}Al MAS NMR spectra of as-made LEV zeolites synthesized at HF/OSDA = 0.5 (bottom), 1.0 (middle), and 2.0 (top). Reproduced with permission from ref. 78. Copyright 2021 Elsevier.
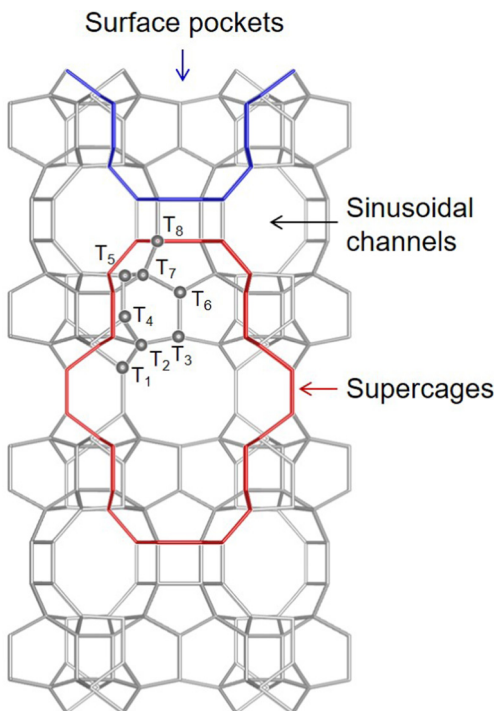
Fig. 4 The MWW structure with eight crystallographically distinct T-sites and three types of pores: supercages, surface pockets, and sinusoidal channels. Adapted from ref. 81.

content (B,Al-MWW, Si/B = ∞, 182–16, Si/Al ∼ 30) were synthesized by adding an appropriate amount (B/Si = 0.0–1.0) of B to an Al-containing synthesis mixture (Si/Al = 30). The degree of deboronation occurred during the calcination and ion-exchange steps to prepare the proton form was quite severe (Si/B = ∞, 484–174), whereas there was no noticeable increase in the Si/Al ratios (∼30). Different B contents in H-B,Al-MWW zeolites had little influence on the strength and density of acid sites, as determined by NH_3-TPD and pyridine-IR. However, the introduction of B atoms regulated the distribution of Brønsted acid sites among the three types of pores in the MWW structure (*i.e.*, supercages, surface pockets, and sinusoidal channels (Fig. 4)). The differentiation of acid sites in 3 different positions was estimated by pyridine-IR through a combination of *m*-xylene transformation and 2,4-dimethylquinoline poisoning, which can deactivate the acid sites in the supercages and the external surface pockets, respectively. With increasing the B/Si ratio in the synthesis mixture from 0.0 to 0.1, the concentration of the Brønsted acid sites in the sinusoidal channels increased compared with those in the supercages and surface pockets. This is probably due to the preferential location of B atoms at T_2 site. However, a further increase in the B/Si ratio in the synthesis mixture relocated most of the Brønsted acid sites into the supercages and surface pockets, due to preferably incorporated B atoms at the T_3, T_8, and T_5 sites and pushed Al atoms to T_6 and/or T_7 sites. In the methanol to hydrocarbons reaction, a linear correlation was observed between the concentration of Brønsted acid sites in the sinusoidal channels of H-B,Al-MWW zeolites and the catalyst lifetime.

B,Al-MFI

Recently, Corma and co-workers reported the manipulation of Al siting in ZSM-5 zeolite by preferentially introducing B atoms at specific T-sites.[83] Theoretical calculations using a series of ZSM-5 zeolite models with different Si/(Al + B) ratios reveal that there is no clear thermodynamic preference for the Al siting at the 12 topologically unique T-sites, but B prefers to occupy the channel intersections (Fig. 1c), especially T_6 site, followed by T_{10} site in the sinusoidal 10-ring channel. The 1-hexene cracking was selected as a test reaction for proving the location of acid sites between within the 10-ring channels and at the channel intersections. Compared to the conventional H-ZSM-5 (Si/Al = 44), the proton form of deboronated B,Al-ZSM-5 (H-B,Al-ZSM-5, Si/B = 82, Si/Al = 46) with similar physicochemical properties displays a low $C_4^=/C_3^=$ ratio. This could be explained by the relatively higher concentration of acid sites located within the 10-ring channels rather than at the intersections. In addition, H-B,Al-ZSM-5 zeolite was more selective to propene in the methanol to propene reaction and showed increased catalytic lifetime. On the other hand, Fan and co-workers found that in ZSM-11 (MEL), a similar structural analogue of MFI, the distribution of acid sites between channels and intersections could also be controlled by introducing an appropriate amount of B atoms.[84,85] The MEL structure consists of two perpendicularly intersecting straight channels along *a*- and *b*-axis.

Sn,Al-MFI

Besides B, the spatial arrangement of Al atoms in ZSM-5 zeolite was tuned by the framework incorporation of Sn. Fan and co-workers prepared Sn-incorporated ZSM-5 zeolites (Si/Sn = 117–424, Si/Al ∼ 95) by varying the concentration of secondary heteroatoms in an aluminosilicate system (Si/Sn = 100–500, Si/Al = 100).[86] Some Sn species contained in the ZSM-5 from the relatively high Sn-containing gel are not fully tetrahedrally coordinated, but exist as extra-framework octahedral Sn species and/or SnO_2 crystal phases. NH_3-TPD and pyridine-IR results showed that the introduction of Sn generated more Lewis acid sites, but had little effect on the strength and amount of Brønsted acid sites. Compared with Sn-free ZSM-5 (Si/Al = 97), the Sn-containing ZSM-5 has a more uniform spatial distribution of Al in the zeolite crystal, an enhanced ratio of paired Al (Co/Al with from 0.22 up to 0.46), and an increased amount of Al atoms located in the 10-ring channels.

Al,Ge-ITH

Fan and co-workers presented the modulation of Al distribution by Ge in ITQ-13 (ITH) zeolite with nine different T-sites.[87] It is well known that the incorporation of Ge, directly below Si in the periodic table, into the silicate zeolites relaxes the geometric constraints in small rings and cages, such as the single 3-ring (*s3r*) and *d4r* units, due to longer average T–O distances and smaller average T–O–T angles than Si.[41,88] The preference of Ge atoms for the T_2 and T_5 sites of the *d4r* units was exploited in competition with the incorporation of

Al atoms. A combination of ^{27}Al and ^{29}Si MAS NMR and DFT calculation results showed that the decrease in the number of Ge atoms per unit cell (56 T-atoms with one Al atom) from 5 to 2 affects the displacement of Al from T_9 site to T_2 and T_5 sites.

At this moment, it is difficult to directly link the thermodynamic competitive siting between Al and other heteroatoms as a decisive factor in determining the Al incorporation at specific T-sites. This is mainly because most of the DFT calculations have been carried out on the simplified zeolite models (not on the real system). For example, the negative charges created by the incorporation of trivalent heteroatoms were normally balanced by inorganic cations (*e.g.*, Na$^+$) or protons, although most zeolite synthesis has been performed in the presence of organic molecules that are also occluded in the final product. In addition, the relative stability of B distributions in more than half of the T-atom sites in B-MWW zeolite models were calculated within 10 kJ mol^{-1},[81] which might not be high enough to make a significant thermodynamic driver for the B incorporation in specific T-sites. This small energy difference provides a possibility that the preferred positions of heteroatoms could be controlled by kinetic factors during the actual crystallization process rather than thermodynamically driven. In line with this, Hong and co-workers reported the synthesis of gallo- and aluminosilicate natrolites (Ga- and Al-NATs) and their *in situ* disorder-order transformation from thermodynamic point of view, which was explained by the intraframework T-atom migration.[89,90] According to the proposed T-atom migration pathway in order to move from metastable disordered state constructed by kinetic origin to a more thermodynamically favorable state, it is inevitable to break the Loewenstein's rule[15] and/or energetically preferential siting of T-atoms during the transformation process. Thus, this supports that the competitive siting between Al and other heteroatoms could be allowed by kinetic control before reaching a thermodynamically more stable state.

Control of the (alumino)silicate network in the initial synthesis mixture

Separate silicon and aluminium source materials

The use of T-atom (T = Si or Al) sources with different reactivity and dissolution rates in alkaline media can kinetically lead to the formation of various (alumino)silicate intermediates (and even quite metastable phases) during the zeolite nucleation and growth.[91] Based on this, it may be reasonable to assume that changes in silicon and aluminium sources influence the incorporation of Al atoms into the zeolite framework.

The effect of Si and Al sources on the Al distribution in the MFI framework was examined by Dedecek and co-workers. A series of high-silica (Si/Al = 12–60) MFI-type zeolites were prepared from synthesis mixtures with a wide range (7–90) of Si/Al ratios in the presence of TPAOH.[92] The distribution of paired framework Al atoms in MFI zeolites was estimated indirectly from the Co^{2+} ion-exchange capacity. There was a
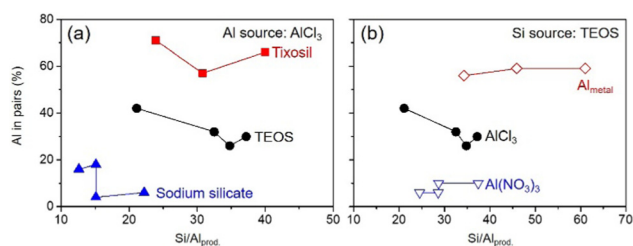
Fig. 5 Effect of (a) silicon and (b) aluminum sources in the synthesis mixtures on the proportion of paired Al in ZSM-5. Adapted from ref. 92.

negligible (<1%) amount of cobalt oxide (Co–O$_x$–Co species) determined by UV-vis spectroscopy ($\sim$30 000 cm^{-1}).

Their comprehensive results show that the degree of Al incorporation and the proportion of paired Al atoms changed according to the combination of various T-atom sources. For example, when using aluminium chloride for MFI synthesis with Si/Al $\sim$ 23, the use of precipitated amorphous silica (Tixosil, Si/Al$_{gel}$ = 30, Co/Al = 0.36) as the Si source led to the highest proportion of Al pairs, compared to tetraethyl orthosilicate (TEOS, Si/Al$_{gel}$ = 30, Co/Al = 0.21) and sodium silicate (Si/Al$_{gel}$ = 60, Co/Al = 0.03) (Fig. 5a). The low proportion of Al pairs in MFI obtained from sodium silicate could be further explained by the presence of Na$^+$ ions stabilizing (alumino)-silicate anionic species in the synthesis mixture. When using TEOS as the Si source for MFI synthesis with Si/Al $\sim$ 32, the replacement of AlCl$_3$ (Si/Al$_{gel}$ = 35, Co/Al = 0.16) by Al metal (Si/Al$_{gel}$ = 30, Co/Al = 0.28) resulted in an increase in the amount of paired Al, whereas the use of aluminium nitrate (Si/Al$_{gel}$ = 30, Co/Al = 0.03) significantly increased the proportion of isolated Al atoms (Fig. 5b).

In another study, four pairs of MFI-type zeolites with similar Si/Al ratios ranging from 13 to 44, but different Al distribution were tested as catalysts for 1-butene cracking reaction.[12] The increase in proximal protons in MFI zeolites showed higher aromatic selectivity in 1-butene conversion by enhancing the oligomerization and hydrogen transfer reactions. Further, the arrangement of proximal protons in H-MFI zeolites with similar Si/Al ratios (13–30), especially located in the channel intersections, led to higher turnover rates in propene oligomerization.[13] This was explained by faster olefin desorption step due to the instability of closely arranged H-bonded olefins and oligomeric alkoxides.

In CHA (Si/Al $\sim$ 15) synthesis using equimolar amounts of TMAdaOH and NaOH, on the other hand, Gounder and co-workers observed that the use of aluminum isopropoxide (Al(O–i–Pr)$_3$) as the Al source more than doubled the proportion of paired Al atoms (Co/Al = 0.22 *vs.* 0.08) compared to Al(OH)$_3$ (Table 1 entries 8 and 9).[14,67] There is insufficient data to understand the influence of different Al sources (or anion species from Al source) on the Al distribution. In order to provide a more universal interpretation of this approach, it may be necessary to analyze the nature of the (alumino)silicate intermediates and the Al concentration profiles (liquid/solid) induced by different T-atom sources (and hydrolysis profiles)

before and during the early stages of hydrothermal treatment, with more examples depending on various framework topologies/compositions and organic SDAs used, *etc.*

Mixing sequence of zeolite ingredients

Dedecek and co-workers showed that the mixing sequence of zeolite ingredients allowed the control of the Al proximity in the MFI framework by inducing the different pathways in the formation of (primary) amorphous precursors.[93] The main difference between the two prepared initial gels with Si/Al = 30 is the input order of the Al source. One is the pre-organization of the aluminosilicate species before adding the TPA$^+$ ions as an organic SDA (*i.e.*, AlCl$_3$–TEOS–TPAOH). The other is the addition of the Al source into the mixture containing TEOS and TPA$^+$ ions (*i.e.*, TEOS–TPAOH–AlCl$_3$) (Fig. 6a). In both sequences, TEOS was dissolved in ethanol and the others in H$_2$O prior to mixing. No additional steps were mentioned in this paper to remove ethanol from the final synthesis mixture. The degree (Si/Al = 21 *vs.* 25) of Al incorporation into the MFI framework was slightly lower in the latter gel, but the amount (Co/Al = 0.21 *vs.* 0.35) of paired Al was 1.5 times higher. The degree of aluminosilicate network in the dried initial gels was investigated by ^{13}C, ^{29}Si, and ^{27}Al MAS NMR spectroscopy. The authors suggest that the pre-formation of the siliceous/TPA$^+$ composite in the latter gel resulted in the generation of relatively abundant Al regions. These Al-rich zones are thought prone to create the aluminosilicate species containing proximal Al atoms, and subsequently rearranged near the TPA$^+$ to balance the positive charge during the (pre)crystallization process.

On the other hand, additional synthesis tests may need to be performed under longer aging times (>90 min) prior to hydrothermal treatment, which may lead to a more thermodynamically homogeneous (alumino)silicate network, negating the mixing order effect. A more detailed monitoring of the evolution of the aluminosilicate network in early solid products and the Si and Al yields will help to clarify the underlying mechanism. Nevertheless, this work implies that the formation of anomalous Al-rich zones in the synthesis mixture may open a pathway to (kinetically) control the Al incorporation.

The possibility of changes in the (alumino)silicate network according to the mixing sequence of zeolite components might be supported by recent studies on the synthesis of aluminosilicate CHA- and AEI-type zeolites reported by Sano and co-workers.[94,95] Unlike the conventional one-step gel preparation, the authors prepared the initial gels in two steps: forming an Al-rich aluminosilicate gel with high alkalinity, then adding an additional Si source and organic SDA to adjust the final gel composition. The (alumino)silicate species with cationic adducts in the liquid phase were separated before and during the induction period of hydrothermal treatment, and monitored based on electrospray-ionization mass spectrometry. Synthesis mixtures prepared *via* the stepwise method provided a broader distribution of oligomers including more condensed species. This was suspected to have beneficial effects on the crystallization of certain zeolites in addition to higher crystallinity and faster crystallization rates.

Amorphous precursors as starting materials

Another strategy to achieve a controlled distribution of heteroatoms in the resulting zeolites and related materials is based on the preformation of amorphous precursors. Yamamoto and co-workers were the first to apply the mechanochemical reaction between SiO$_2$ and a source of substitution metal (*e.g.*, metal oxide or metal hydroxide) for the preparation of amorphous metallosilicate precursors.[96] The subsequent hydrothermal treatment of prepared amorphous metallosilicates as
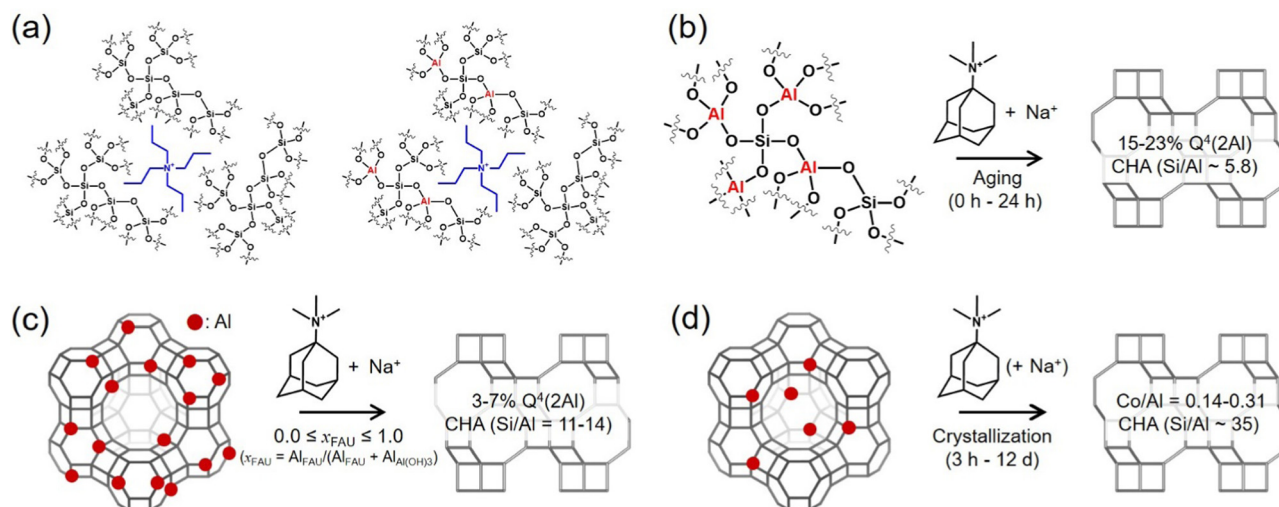
Fig. 6 Control of the (alumino)silicate network. (a) Amorphous (alumino)silicate networks according to the mixing sequence of zeolite ingredients: pre-formed silicate/TPA$^+$ composite before adding the Al source (left; order: TEOS–TPAOH–AlCl$_3$) and conventional aluminosilicate/TPA$^+$ composite (right; order: AlCl$_3$–TEOS–TPAOH). Refers to the approach in ref. 93. Synthesis of CHA-type zeolites from (b) Al-rich (Si/Al = 2.5) amorphous aluminosilicate precursors (refers to ref. 103), (c) Al-rich (Si/Al = 2.8) crystalline FAU-type zeolite (refers to ref. 115), and (d) Si-rich (Si/Al = 40) crystalline FAU-type zeolite (refers to ref. 11) as starting materials.

starting reagents for both Si and heteroatom (*e.g.*, Ti, Sn, Ga, Fe) sources in the presence of organic SDAs led to various metal-substituted zeolites.[96–102] Muramatsu and co-workers showed that the use of amorphous metallosilicates affects the uniform distribution of heteroatoms in the final metal-substituted MFI-type zeolites, compared to those synthesized *via* the conventional one-pot hydrothermal process using soluble starting reagents (*e.g.*, TEOS and metal nitrates).[100–102] They stated that the uniformly distributed heteroatoms could be attributed to the chemical potentials of the Si and heteroatom sources remaining constant in the liquid phase during the hydrothermal process. This was explained by partially dissolved polymetallosilicate intermediates (*i.e.*, Si–O–metal species) from the amorphous metallosilicate precursors under the control of the solid–liquid equilibrium. They also suggested that preformed Si–O–metal species dissolved in the liquid phase made the condensation rates between Si and heteroatom species negligible, assisting to form the desired zeolites. This approach may require careful control of the pre-aging (or pre-dissolution) step to prevent the pre-organized amorphous precursors with potential for kinetic differences from re-organizing a more thermodynamically preferred state in liquid phase.

Following this work, the same group applied this strategy to control the paired Al content in CHA-type aluminosilicate zeolites under seed-assisted (5 wt% CHA-seeds based on total weight of SiO_2) conditions.[103] An Al-rich (Si/Al = 2.5) amorphous aluminosilicate precursor was prepared *via* a polymerized complex method using propylene glycol-modified silane and $Al(NO_3)_3$ as starting materials (Fig. 6b). Although the broad asymmetric signal around −105 ppm in the ^{29}Si MAS NMR spectrum of X-ray amorphous solid made it difficult to assign $Q^4(nAl)$ species, the prepared amorphous precursor as a source of both Al and Si could be considered to statistically contain large amounts of $Q^4(2Al)$ units due to its high Al content. When the initial Si/Al ratio in the synthesis mixture was fixed to 10, they succeeded in synthesizing a series of CHA-type zeolites (Si/Al = 5.7–5.8) with controlled proportion (15–23%) of $Q^4(2Al)$ to the total Al-containing $Q^4(nAl)$ species. It was found to be kinetically tunable by altering the exposure (aging) time (0–24 h) of the amorphous precursor to the basic synthesis mixtures (here, TMAdaOH and NaOH with $OH^-/Si = 0.64$). It was hypothesized to affect the degree of hydrolysis and dissolution of desirable units prior to hydrothermal treatment. In this regard, experimental evidence describing the structure of (alumino)silicate units dissolved in liquid phase or actually participating in structural growth, as well as their concomitant rearrangement and condensation, would help extend this strategy.

Crystalline zeolites as starting materials

Interzeolite conversion (and in a way seed-assisted) approaches for zeolite synthesis are based on the metastable nature of pre-crystallized zeolites under the crystallization conditions and their transformation into other phases through dissolution/recrystallization processes.[39,104,105] It was in the late 1940s when Barrer first used such zeolite synthesis, allowing the

synthesis of new aluminosilicate zeolite (KFI) from analcime (ANA) in the presence of Ba^{2+}.[106] Since the early 2010s, this strategy has been extensively studied in the presence and absence of organic SDAs, providing high selectivity for specific structure types of zeolites and accelerating the rate of zeolite crystallization. In addition, it has been found to be beneficial for expanding the compositional range of crystalline microporous materials. For example, CHA-type zeolites with a wide range of Si/Al ratios (2 to 67) were synthesized *via* the interzeolite conversion of FAU with or without organic SDAs (*e.g.*, TMAda$^+$, *N,N,N*-trimethylbenzylammonium, tetraethylammonium).[39,107–111] Especially, the lower limit of Al incorporation in CHA zeolite was not achievable through the conventional synthesis using amorphous/soluble Si and Al sources. Interestingly, two novel zeolite structures, YNU-5 (YFI) and PST-33 (PTT), were recently discovered by the interzeolite conversion of FAU, used as an Al source, in the presence of dimethyldipropylammonium and 5-azonia-spiro[4.4]nonane as organic SDAs, respectively.[112–114] Both structures did not crystallize from classical amorphous/soluble Si and Al sources.

Al-rich FAU (Si/Al = 2.8) to CHA (Si/Al ∼ 11–14). Recently, this interzeolite conversion method has been extended to control the Al distribution in zeolite framework. Yokoi and co-workers investigated the effect on Al distribution in the CHA framework using FAU-type zeolite (Si/Al = 2.8) as (partial) Al source together with $Al(OH)_3$ ($x_{FAU} = Al_{FAU}/(Al_{FAU} + Al_{Al(OH)3})$) (Fig. 6c).[115] To keep the Si/Al ratio constant at 10, they used fumed silica as an additional Si source in the TMAda$^+$–Na$^+$-containing initial synthesis gel with calcined SSZ-13 (CHA, Si/Al = 7.7, 5 wt%) seed crystals. Regardless of x_{FAU} in the synthesis mixtures, all syntheses always yielded CHA-type zeolites, but the solid yield and the Al content in zeolites decreased with increasing x_{FAU}. The ^{29}Si MAS NMR spectra of calcined samples showed when CHA-type zeolites with similar Si/Al ratios (∼11 from $0.1 \leq x_{FAU} \leq 0.5$ and ∼14 from $0.75 \leq x_{FAU} \leq 0.1$) were synthesized from higher x_{FAU} ratios, the proportion of $Q^4(2Al)$ species tended to increase (3.1 to 7.3% and 5.8 to 7.0%, respectively), whereas the opposite trend was observed for the proportion of $Q^4(1Al)$ species. Since the ^{29}Si resonances associated with $Q^4(nAl)$ sites generate based on the number of next-nearest neighbour Al atoms, additional experiment (*e.g.*, titration by divalent metal cations) is thus required, in order to quantify 6MR proximate Al sites with Al–O–(Si–O)$_2$–Al sequence. However, the results clearly show that the use of crystalline zeolite as the Al source affects the Al distribution in the resulting zeolites, despite not having enough data to explain the dissolution/recrystallization mechanism of starting material. In the methanol to olefins reaction, the catalytic lifetime decreased with increasing $Q^4(2Al)$ species in H-CHA zeolites with almost identical Si/Al ratio ∼ 11 due to the coke deposits, while the product selectivity was hardly affected.

The feasibility of directly tuning the Al distribution in a particular structure type of zeolites *via* the interzeolite conversion method can be supported by the results of Okubo and co-workers with the help of both experimental and statistical approaches.[116] They calculated the proportion of $Q^4(nAl)$

species using 10 000 independently randomly distributed Al atoms in theoretical CHA models with Si/Al ratios of 2.20 and 2.56, respectively, and compared them with the experimentally observed values. The results revealed that the non-random nature of Al distribution in CHA (Si/Al = 2.20) derived from the interzeolite conversion of FAU (Si/Al = 2.7) as the sole Si and Al source in a KOH solution without any organic SDAs is more evident than for the same materials (Si/Al = 2.56) prepared by conventional synthesis from amorphous/soluble Si and Al sources. Especially, the fraction of Q^4(2Al) of the former CHA deviated the most from the statistical average and belonged to the upper range of outliers. In addition, the relative energy calculations on CHA models possessing Si speciation closest to experimental ^{29}Si NMR data in the presence of K^+ cations, counterbalancing AlO_4^- tetrahedra in the framework, exhibited that CHA derived from FAU is more energetically preferred to the counterparts with random Al locations. These results suggest that the interzeolite conversion method here for very aluminous products appears to be useful for controlling the distribution of heteroatom in zeolite framework when appropriately combining with inorganic/organic SDAs with properly selected type/amount of starting crystalline materials.

High-silica FAU (Si/Al = 40) to CHA (Si/Al ~ 35) and MFI (Si/Al ~ 36). Dusselier and co-workers investigated the synthetic details of the interzeolite conversion strategy for high silica materials. They aimed at tuning the Al distribution in zeolite frameworks by systematically controlling the synthesis parameters such as starting material type, initial gel composition, and crystallization temperature and time.[11] In an alkali-free, TMAda$^+$-containing synthesis, the use of USY (FAU, Si/Al = 40) without additional Si and Al sources led to the crystallization of high-silica SSZ-13 (Si/Al ~ 35) with a remarkably high content

(Co/Al = 0.31) of proximate Al in 6MRs in the CHA topology (Fig. 6d and 7a). The proximate Al sites were counted from titration by Co^{2+} cations (*i.e.*, divalent cation capacity (DCC) defined as the Co/Al ratio). When using ZSM-5 (Si/Al = 40) instead of USY under the same conditions, however, the DCC of the crystallized SSZ-13 (Si/Al ~ 26) was significantly lower (0.06). This is probably due to the different dissolution kinetics of the starting zeolite. In addition, this high DCC obtained *via* the interzeolite conversion from USY could not be easily achieved using a conventional amorphous aluminosilicate gel with the identical oxide composition (Co/Al = 0.0) (Table 1 entries 12, 14 and 15). It is also noteworthy that this DCC value (0.31) is sufficiently high to be comparable with that (0.22) of the relatively Al-rich SSZ-13 (Si/Al = 14–18) prepared from the conventional procedure involving the use of TMAda$^+$ and Na$^+$ as SDAs.[14] On the other hand, the α-Fe(II) species, which are the active sites of the methane partial oxidation reaction, were more hosted in Fe-exchanged SSZ-13 (Si/Al ~ 35) with higher DCC values, influencing higher amounts of methanol production.[11]

Of particular interest is that after obtaining (starting from USY and heating at 160 °C) a fully crystallized high-silica SSZ-13 with the highest Co^{2+} uptake (DCC = 0.31) after 3 h, the DCC value began to drop continuously with prolonged hydrothermal treatment (Fig. 7a). After 12 days (288 h) of heating, the DCC decreased to less than 50% (0.14) without significant change in the bulk Si/Al ratio (~34). This trend was more pronounced at higher crystallization temperature (>160 °C) (Fig. 7b). In the long-term crystallization study at 180 °C for 12 days under the same interconversion system, a higher amount of isolated Al sites (Co/Al = 0.07) in SSZ-13 with similar Al content (Si/Al ~ 31) was obtained.
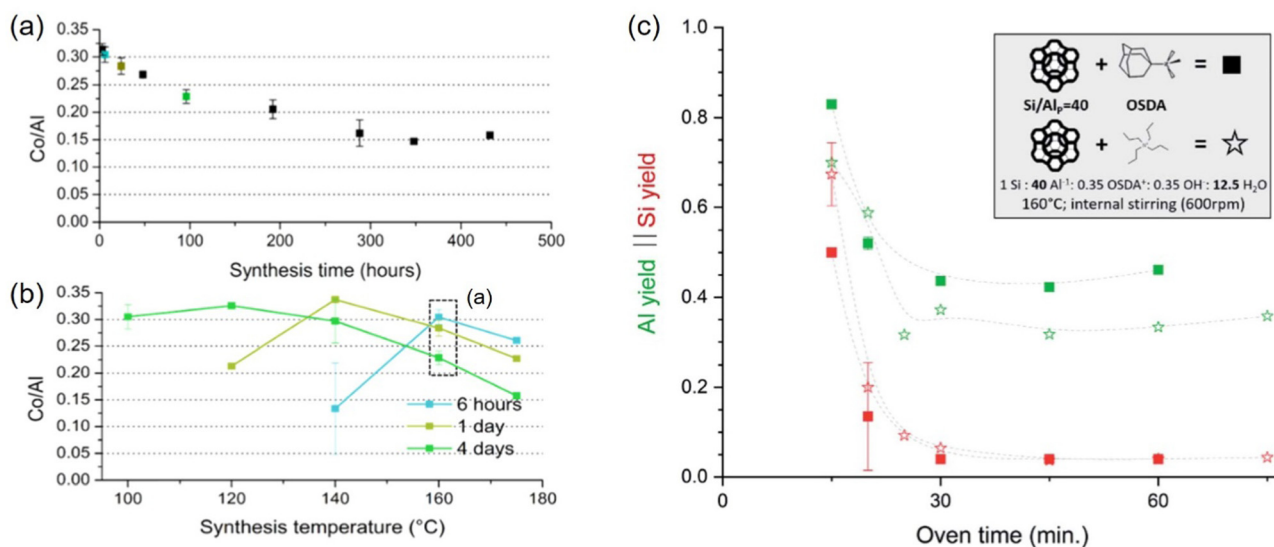
Fig. 7 Effect of (a) synthesis time at 160 °C and (b) synthesis temperatures and time on the change of proximate Al sites (Co/Al ratio) in SSZ-13 zeolites (CHA, Si/Al ~ 35) synthesized from USY (FAU, Si/Al = 40) without additional Si or Al sources in the presence of TMAda$^+$ in the alkali-free interzeolite conversion system. Reproduced with permission from ref. 11. Copyright 2019 American Chemical Society. (c) Incongruent dissolution behavior of USY during the dissolution stage in the alkali-free interzeolite conversion systems for CHA and MFI synthesis in the presence of TMAda$^+$ and TPA$^+$, respectively. Reproduced with permission from ref. 123. Copyright 2021 Royal Society of Chemistry.

The same phenomenon was also found in our recent study on the synthesis of MFI-type zeolite (Si/Al ∼ 36) prepared by interzeolite conversion of USY in the TPA⁺–Na⁺ system.[117] The DCC values for fully crystalline MFI steadily decreased from 0.19 (2 h) to 0.06 (288 h). The *in situ* rearrangement of proximate Al into isolated Al observed during their crystallization process (even after full crystallinity is reached) was rationalized from a thermodynamic point of view. It might be driven by repulsive Coulomb interactions between negatively charged AlO_4^- tetrahedral units in the zeolite framework, according to Dempsey's and Loewenstein's rules.[16,118] However, higher energy inputs (*e.g.*, longer synthesis times and higher temperatures) are required along with a high degree of framework flexibility to overcome the barrier and induce the intraframework Al migration.

Contrary to the trend found in these two cases, a series of fully crystalline CHA (Si/Al ∼ 35) synthesized from the interzeolite conversion of USY in the TMAda⁺–Na⁺ system retained their DCC (Co/Al ∼ 0.25) during prolonged heating from 2 h to 4 days in the crystallization medium (Table 1 entry 13).[117] This could be explained by the limited mobility of the inorganic and/or organic SDAs balanced with the negative framework charges. In other words, the immovable Al siting might be energetically driven by the nature of the position occupied by SDAs.

Recent studies seem to show that the long-postulated theory for successful interzeolite conversion, namely the structural similarity between the starting (parent) and final (daughter) zeolites, is not an important prerequisite.[109,119–122] Therefore, it is difficult to interpret that the specific atomic arrangement containing the adjacent Al atoms of the parent material was directly supplied to crystallize the daughter zeolites. Through the kinetic (temporal) analysis of the entire interconversion process, our group proposed two main kinetic factors in creating abnormally high DCC values in the resulting (not-thermodynamically equilibrated) zeolites: (i) the formation of Al-rich residual solids during the dissolution stage (incongruent dissolution, Fig. 7c) and (ii) rapid kinetic assembly through non-classical growth instead of classical monomer addition.[11,117,123] The above studies clearly demonstrated that the interzeolite conversion can be an efficient way to prepare zeolites with finely controlled Al distribution through a combination of kinetic and thermodynamic control. To realize the broader applicability of this approach, further mechanistic elucidation of interzeolite conversions, especially at the assembly stage, is still required, as well as an expansion of the control in these systems to wider Si/Al ranges in the products.

Conclusions

In this Feature Article we describe recent attempts to tailor the chemical properties of zeolites by tuning the Al distribution through bottom-up synthetic approaches. A glance at all these synthetic strategies reveals that the unique arrangement of Al atoms in zeolites can be feasible by (i) controlling or aiming toward the energetically preferential Al sites and (ii) forming specific (alumino)silicate networks and controlling their reactivity and/or dissolution rates. We analyze them using a kinetic *vs.* a thermodynamic approach, bearing in mind that the distinction is not strict and the interpretation of those terms depends on the timescale.

Energetically preferential Al siting at desired locations in the zeolite framework could be induced by creating new geometric and/or electrostatic interactions between negatively charged framework units and organic/inorganic SDAs. In addition, the second tri- or tetravalent heteroatom (*e.g.*, B, Sn, Ge) has a thermodynamic preference for a particular T-site due to its different average T–O distance and T–O–T angle from Si (or Al), which could be exploited in competition for Al incorporation (Fig. 8, left). These two concepts were demonstrated by introducing appropriately selected extra-framework components and other heteroatoms into the initial mixture, further allowing the Al distribution within the zeolite framework to be predicted (to some extent) and designed. However, considering that hydrothermal zeolite synthesis occurs in very complex synthesis media and involves a number of chemical interactions, the kinetic control might be more significantly involved in the actual crystallization process.

Specific (alumino)silicate networks could be formed through *in situ* by changing the Si and Al sources and changing the mixing order of zeolite ingredients, as well as *ex situ* using preformed amorphous and crystalline (alumino)silicate precursors (Fig. 8, right). Controlled (alumino)silicate networks are thought to have different dissolution behaviours that influence the properties of the dissolved (or re-organized) (alumino)silicate species in the liquid phase. The formation of anomalous Al-rich zones in the synthesis mixture before or during the early (dissolution) stage of hydrothermal treatment may be one of the important factors for obtaining zeolites containing proximate Al sites. Especially, the distribution of proximal Al sites in some resulting zeolites was kinetically controllable depending on the pre-aging (or pre-dissolution) time of the (alumino)silicate precursors and/or additional crystallization time after obtaining a fully crystalline final product.
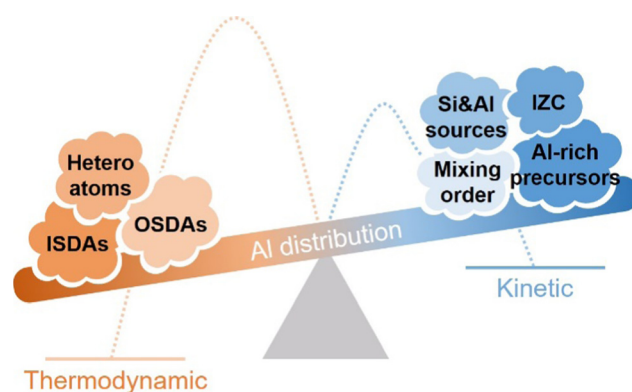
Fig. 8 Schematic representation of synthetic strategies with their tentative division along a thermodynamic or more kinetic control to steer the Al distribution in zeolites. ISDA and OSDA are inorganic and organic structure directing agents, respectively. IZC is interzeolite conversion method.

A further understanding of the precise roles of various components and their interplay in synthesis mixtures (on dissolution/aging/growth) is still needed to obtain fine-tuned catalysts and develop efficient strategies available for diverse zeolite framework structures and/or compositions. Nevertheless, a lot of progress has been made in the last decade and it is clear that the proper selection and combination of the synthetic approaches introduced above will provide guidance for the preparation of zeolites with tailored Al-derived properties.

Perspectives and outlook

Amorphous and crystalline (alumino)silicate precursors as starting materials are expected to have different reactivity and dissolution rates in alkaline media depending on their physico-chemical properties, such as (local micro)structure and composition. Provided that aging is not long or harsh (*i.e.*, avoiding an equilibrium state which is independent of the starting sources) different (alumino)silicate networks will affect the distribution and structure of (alumino)silicate species dissolved in the liquid phase, as well as the formation of 'abnormal' regions (*e.g.*, Al-rich zone). In this respect, the use of properly engineered precursors as the starting materials (and fast syntheses) can allow distinctive zeolite crystallization pathways compared to conventional synthesis starting from amorphous/soluble Si and Al sources. Additionally, changes in the chemical environment of the synthesis medium in which the initial precursors dissolve or transform can affect the properties of the intermediate materials, which in turn can influence on the final product and its properties. The underlying mechanism is somewhat unclear, but the principle has been demonstrated in several related studies.

Muramatsu's group investigated the effect of (alumino)-silicate network in the initial synthesis mixture on the crystallization of MOR-type zeolites while keeping the molar composition the same (Si/Al/NaOH/H$_2$O = 1/0.05/0.44/30).[124] They employed various Al and Si sources, ranging from homogeneous staring reagents (*e.g.*, Al(NO$_3$)$_3$ and TEOS) to three prepared amorphous precursors with Si/Al = ∞, 2, and 20, denoted as AP, AP2, and AP20, respectively. Among them, MOR-type zeolites with Si/Al ratios of up to 13 were produced only from amorphous aluminosilicate precursors (*i.e.*, AP2 and AP20). Especially, the use of Al-rich AP2 precursors together with additional Si source improved the crystallization rate. This is presumably due to the presence of abundant penta-coordinated Al species, which has been reported to dissolve more readily than tetra- and hexa-coordinated ones commonly found in aluminas and aluminosilicates.[125]

Wakihara and co-workers reported similar observations in the synthesis of AEI-type zeolites by applying amorphous aluminosilicate precursors.[126] The initial amorphous precursors were prepared by mixing colloidal silica and sodium aluminate under alkaline conditions at room temperature for 24 h. The authors modified the amorphous precursors by dealumination with a 0.4 M H$_2$SO$_4$ solution. The properties of the modified precursors were compared with those of the initial ones using ^{27}Al MAS NMR and UV Raman spectroscopies and X-ray pair distribution function analysis. Dealumination could not only change the Si/Al ratio (from 4.6 to 14–25), but also alter the aluminium states and the T–O connectivity in the amorphous precursors. This made the amorphous precursors relatively unstable and reactive in alkaline synthesis mixtures and allowed the formation of AEI-type zeolite with a Si/Al ratio of 6.6 in the presence of *N*,*N*-dimethyl-3,5-dimethylpiperidinium hydroxides as an organic SDA. We should note that the aluminosilicate AEI zeolite is typically synthesized using at least in part FAU-type zeolites.[39,104,127,128]

Another role of manipulated precursors is based on facilitating zeolite nucleation within as well as on the surface of the amorphous precursors. This concept differs slightly from the former cases where it was claimed that the resulting zeolite began to grow at the crystal–liquid interface through the supply of desired (alumino)silicate species at the expense of amorphous precursors as starting reagents. Rimer and co-workers showed that alkali (K$^+$ or Na$^+$)-infused amorphous precursors reduced the crystallization time by more than 50% for LTL-, MOR-, and CHA-type zeolites compared to synthesis using as-received fumed silica, whereas there was little impact on the synthesis of MFI-type zeolite.[105,129,130] Although the exact effect of alkali-infused amorphous silica on enhancing the rates of crystal formation remains elusive, they explained the presence of alkali metal inside the amorphous silicates could act as an inorganic SDA and promote particle aggregation.

Recently, Linares and García-Martínez reported the synthesis of hierarchical catalysts whose mesoporosity and acidity evolved during partial interzeolite conversion of FAU into *BEA.[131] Three different synthesis media were prepared from (i) the parent FAU zeolite (Si/Al = 15.5) in the presence of TEAOH, (ii) an uncalcined surfactant (CTAB)-templated FAU zeolite (Si/Al = 16.0) with TEAOH, and (iii) the parent FAU zeolite with a mixture of TEAOH and CTAB. In the intermediate stage of all three media, amorphous mesoporous intermediates containing zeolite building units were formed, and their textural properties and consequent catalytic performance involving large molecules were tuned over time. In particular, the last two media using surfactants helped develop well-defined mesopores in amorphous intermediate solids. However, the presence of CTAB in the synthesis mixture delayed the kinetics of amorphization of FAU zeolite (0.5 *vs.* 0.5 *vs.* 2 days) and growth of *BEA zeolite (*ca.* 100% *BEA crystallinity: 1.5 day *vs.* 2 day *vs.* > 8 day). Moreover, the direct addition of CTAB to the initial mixture affected the desilication kinetics during the dissolution stage, leading to the formation of amorphous intermediate with lower Al content (Si/Al = 8.8 *vs.* 8.1 *vs.* 13.2).

An understanding of crystallization mechanisms, in particular the dissolution, rearrangement, and condensation behaviour of desired units containing Al atoms, will lead to proper preparation of preformed precursors and synthesis media for the zeolites with desired chemical properties (here, Al site content and location control). However, this is quite complicated due to the multiple crystallization pathways that occur in

complex synthesis media composed of many solid and liquid species and the occurrence of steps in parallel (*e.g.*, nucleation and growth) as well as thermal equilibration when given time. In addition, the lack of long-range, XRD-detectable (periodic) order makes it difficult to experimentally determine the exact microstructure of amorphous precursors, especially in reactive conditions. Various synthetic (and transient) parameters such as organic and inorganic SDAs and alkalinity can also continuously affect the structural rearrangement in this metastable phase during the induction period. These restrict finding the connections between the starting materials and the resulting zeolites.

Nevertheless, several papers introduced in this Feature Article clearly demonstrate the differences between the starting materials in terms of the synthesis outcomes, with concomitant effects on the heteroatom distribution as well as the kinetic benefits of crystallization. Subtle changes in physicochemical properties of amorphous and crystalline precursors and the chemical environment of the synthesis medium where dissolution and/or transformation occurs can potentially form another abnormal aluminosilicate network. This may be one of the possible ways to activate kinetic factors to control the Al incorporation in zeolites before entering an energetically stable state.

Author contributions

J. B. wrote the review with critical input and corrections from M. D.

Conflicts of interest

There are no conflicts to declare.

Acknowledgements

References

1 M. E. Davis, *Nature*, 2002, **417**, 813–821.
2 T. F. Degnan Jr, *J. Catal.*, 2003, **216**, 32–46.
3 W. Vermeiren and J.-P. Gilson, *Top. Catal.*, 2009, **52**, 1131–1161.
4 L. Čapek, J. Dědeček, B. Wichterlová, L. Cider, E. Jobson and V. Tokarová, *Appl. Catal., B*, 2005, **60**, 147–153.
5 L. Čapek, J. Dědeček, P. Sazama and B. Wichterlová, *J. Catal.*, 2010, **272**, 44–54.
6 J. Dědeček, L. Čapek, P. Sazama, Z. Sobalík and B. Wichterlová, *Appl. Catal., A*, 2011, **391**, 244–253.
7 P. Sazama, N. K. Sathu, E. Tabor, B. Wichterlová, Š. Sklenák and Z. Sobalík, *J. Catal.*, 2013, **299**, 188–203.
8 U. Deka, I. Lezcano-Gonzalez, B. M. Weckhuysen and A. M. Beale, *ACS Catal.*, 2013, **3**, 413–427.
9 C. Paolucci, A. A. Parekh, I. Khurana, J. R. Di Iorio, H. Li, J. D. Albarracin Caballero, A. J. Shih, T. Anggara, W. N. Delgass, J. T. Miller, F. H. Ribeiro, R. Gounder and W. F. Schneider, *J. Am. Chem. Soc.*, 2016, **138**, 6028–6048.
10 T. Ryu, N. H. Ahn, S. Seo, J. Cho, H. Kim, D. Jo, G. T. Park, P. S. Kim, C. H. Kim, E. L. Bruce, P. A. Wright, I.-S. Nam and S. B. Hong, *Angew. Chem., Int. Ed.*, 2017, **56**, 3256–3260.
11 J. Devos, M. L. Bols, D. Plessers, C. V. Goethem, J. W. Seo, S.-J. Hwang, B. F. Sels and M. Dusselier, *Chem. Mater.*, 2020, **32**, 273–285.
12 P. Sazama, J. Dědeček, V. Gábová, B. Wichterlová, G. Spoto and S. Bordiga, *J. Catal.*, 2008, **254**, 180–189.
13 M. Bernauer, E. Tabor, V. Pashkova, D. Kaucký, Z. Sobalík, B. Wichterlová and J. Dedecek, *J. Catal.*, 2016, **344**, 157–172.
14 J. R. Di Iorio, C. T. Nimlos and R. Gounder, *ACS Catal.*, 2017, **7**, 6663–6674.
15 S. Nystrom, A. Hoffman and D. Hibbitts, *ACS Catal.*, 2018, **8**, 7842–7860.
16 W. Loewenstein, *Am. Mineral.*, 1954, **39**, 92–96.
17 J. H. Kwak, H. Zhu, J. H. Lee, C. H. F. Peden and J. Szanyi, *Chem. Commun.*, 2012, **48**, 4758–4760.
18 F. Giordanino, P. N. R. Vennestrøm, L. F. Lundegaard, F. N. Stappen, S. Mossin, P. Beato, S. Bordiga and C. Lamberti, *Dalton Trans.*, 2013, **42**, 12741–12761.
19 J. A. van Bokhoven, D. C. Koningsberger, P. Kunkeler, H. Van Bekkum and A. P. M. Kentgens, *J. Am. Chem. Soc.*, 2000, **122**, 12842–12847.
20 S. Sklenak, J. Dědeček, C. Li, B. Wichterlová, V. Gábová, M. Sierka and J. Sauer, *Angew. Chem., Int. Ed.*, 2007, **46**, 7286–7289.
21 Z. J. Berkson, M. F. Hsieh, S. Smeets, D. Gajan, A. Lund, A. Lesage, D. Xie, S. I. Zones, L. B. McCusker, C. Baerlocher and B. F. Chmelka, *Angew. Chem., Int. Ed.*, 2019, **58**, 6255–6259.
22 M. B. Schmithorst, S. Prasad, A. Moini and B. F. Chmelka, Presented in part at the 20th International Zeolite Conference 2022, Valencia, Spain, July, 2022.
23 L. R. Aramburo, Y. Liu, T. Tyliszczak, F. M. de Groot, J. C. Andrews and B. M. Weckhuysen, *ChemPhysChem*, 2013, **14**, 496–499.
24 A. B. Pinar, L. Gómez-Hortigüela, L. B. McCusker and J. Pérez-Pariente, *Chem. Mater.*, 2013, **25**, 3654–3661.
25 K. Muraoka, W. Chaikittisilp, T. Yanaba, T. Yoshikawa and T. Okubo, *Angew. Chem., Int. Ed.*, 2018, **57**, 3742–3746.
26 A. B. Pinar, P. Rzepka, A. J. Knorpp, L. B. McCusker, C. Baerlocher, T. Huthwelker and J. A. van Bokhoven, *J. Am. Chem. Soc.*, 2021, **143**, 17926–17930.
27 J. A. van Bokhoven, T.-L. Lee, M. Drakopoulos, C. Lamberti, S. Thieß and J. Zegenhagen, *Nat. Mater.*, 2008, **7**, 551–555.
28 A. Vjunov, J. L. Fulton, T. Huthwelker, S. Pin, D. Mei, G. K. Schenter, N. Govind, D. M. Camaioni, J. Z. Hu and J. A. Lercher, *J. Am. Chem. Soc.*, 2014, **136**, 8296–8306.
29 R. Bohinc, J. Hoszowska, J.-C. Dousse, W. Błachucki, F. Zeeshan, Y. Kayser, M. Nachtegaal, A. B. Pinar and J. A. van Bokhoven, *Phys. Chem. Chem. Phys.*, 2017, **19**, 29271–29277.
30 J. Dědeček, D. Kaucký and B. Wichterlová, *Chem. Commun.*, 2001, 970–971.
31 J. Dědeček, E. Tabor and S. Sklenak, *ChemSusChem*, 2019, **12**, 556–576.
32 M. Bocus, S. E. Neale, P. Cnudde and V. Van Speybroeck, *Reference Module in Chemistry, Molecular Sciences and Chemical Engineering*, Elsevier, Inc, Amsterdam, 2021.
33 R. M. Barrer and P. J. Denny, *J. Chem. Soc.*, 1961, 971–982.
34 R. Szostak, *Handbook of Molecular Sieves*, Van Nostrand Reinhold, New York, 1992.
35 C. S. Blackwell, R. W. Broach, M. G. Gatter, J. S. Holmgren, D. Y. Jan, G. J. Lewis, B. J. Mezza, T. M. Mezza, M. A. Miller, J. G. Moscoso, R. L. Patton, L. M. Rohde, M. W. Schoonover, W. Sinkler, B. A. Wilson and S. T. Wilson, *Angew. Chem., Int. Ed.*, 2003, **42**, 1737–1740.
36 M. A. Miller, J. G. Moscoso, S. C. Koster, M. G. Gatter and G. J. Lewis, *Stud. Surf. Sci. Catal.*, 2007, **170**, 347–354.
37 M. Moliner, F. Rey and A. Corma, *Angew. Chem., Int. Ed.*, 2013, **52**, 13880–13889.
38 Q. Ke, T. Sun, H. Cheng, H. Chen, X. Liu, X. Wei and S. Wang, *Chem. – Asian J.*, 2017, **12**, 1043–1047.

39 M. Dusselier and M. E. Davis, *Chem. Rev.*, 2018, **118**, 5265–5329.

40 J. Shin, D. Jo and S. B. Hong, *Acc. Chem. Res.*, 2019, **52**, 1419–1427.

41 M. Shamzhy, M. Opanasenko, P. Concepción and A. Martínez, *Chem. Soc. Rev.*, 2019, **48**, 1095–1149.

42 A. Palčić and V. Valtchev, *Appl. Catal., A*, 2020, **606**, 117795.

43 R. Simancas, A. Chokkalingam, S. P. Elangovan, Z. Liu, T. Sano, K. Iyoki, T. Wakihara and T. Okubo, *Chem. Sci.*, 2021, **12**, 7677–7695.

44 S. Wang, Y. He, W. Jiao, J. Wang and W. Fan, *Curr. Opin. Chem. Eng.*, 2019, **23**, 146–154.

45 T. T. Le, A. Chawla and J. D. Rimer, *J. Catal.*, 2020, **391**, 56–68.

46 E. E. Bickel, C. T. Nimlos and R. Gounder, *J. Catal.*, 2021, **399**, 75–85.

47 H. Gies and B. Marker, *Zeolites*, 1992, **12**, 42–49.

48 R. F. Lobo, S. I. Zones and M. E. Davis, *J. Incl. Phenom. Macrocycl. Chem.*, 1995, **21**, 47–78.

49 J. Li, A. Corma and J. Yu, *Chem. Soc. Rev.*, 2015, **44**, 7112–7127.

50 D. Schwalbe-Koda, S. Kwon, C. Paris, E. Bello-Jurado, Z. Jensen, E. Olivetti, T. Willhammar, A. Corma, Y. Román-Leshkov, M. Moliner and R. Gómez-Bombarelli, *Science*, 2021, **374**, 308–315.

51 A. B. Pinar, R. Verel, J. Pérez-Pariente and J. A. van Bokhoven, *Microporous Mesoporous Mater.*, 2014, **193**, 111–114.

52 A. B. Pinar, C. Márquez-Álvarez, M. Grande-Casas and J. Pérez-Pariente, *J. Catal.*, 2009, **263**, 258–265.

53 L. Gómez-Hortigüela, A. B. Pinar, F. Corà and J. Pérez-Pariente, *Chem. Commun.*, 2010, **46**, 2073–2075.

54 C. Márquez-Alvarez, A. B. Pinar, R. García, M. Grande-Casas and J. Pérez-Pariente, *Top. Catal.*, 2009, **52**, 1281–1291.

55 Y. Román-Leshkov, M. Moliner and M. E. Davis, *J. Phys. Chem. C*, 2011, **115**, 1096–1102.

56 Q. Ke, I. Khalil, B. Smeyers, Z. Li, R. de Oliveira-Silva, B. Sels, D. Sakellariou and M. Dusselier, *Angew. Chem., Int. Ed.*, 2021, **60**, 24189–24197.

57 F. Delprato, L. Delmotte, J. L. Guth and L. Huve, *Zeolites*, 1990, **10**, 546–552.

58 D. He, D. Yuan, Z. Song, Y. Xu and Z. Liu, *Chin. J. Catal.*, 2019, **40**, 52–59.

59 J. Bae and S. B. Hong, *Chem. Sci.*, 2018, **9**, 7787–7796.

60 L. Lakiss, C. Kouvatas, J. P. Gilson, H. A. Aleksandrov, G. N. Vayssilov, N. Nesterenko, S. Mintova and V. Valtchev, *Angew. Chem., Int. Ed.*, 2021, **60**, 26702–26709.

61 X. Li, H. Han, W. Xu, S. J. Hwang, P. Lu, A. Bhan and M. Tsapatsis, *Angew. Chem., Int. Ed.*, 2022, **61**, e202111180.

62 Y. Sada, S. Miyagi, K. Iyoki, M. Yoshioka, T. Ishikawa, Y. Naraki, T. Sano, T. Okubo and T. Wakihara, *Microporous Mesoporous Mater.*, 2022, 112196.

63 T. Yokoi, H. Mochizuki, S. Namba, J. N. Kondo and T. Tatsumi, *J. Phys. Chem. C*, 2015, **119**, 15303–15315.

64 T. Yokoi, H. Mochizuki, T. Biligetu, Y. Wang and T. Tatsumi, *Chem. Lett.*, 2017, **46**, 798–800.

65 T. Biligetu, Y. Wang, T. Nishitoba, R. Otomo, S. Park, H. Mochizuki, J. N. Kondo, T. Tatsumi and T. Yokoi, *J. Catal.*, 2017, **353**, 1–10.

66 S. Park, T. Biligetu, Y. Wang, T. Nishitoba, J. N. Kondo and T. Yokoi, *Catal. Today*, 2018, **303**, 64–70.

67 J. R. Di Iorio and R. Gounder, *Chem. Mater.*, 2016, **28**, 2236–2247.

68 J. R. Di Iorio, S. Li, C. B. Jones, C. T. Nimlos, Y. Wang, E. Kunkes, V. Vattipalli, S. Prasad, A. Moini, W. F. Schneider and R. Gounder, *J. Am. Chem. Soc.*, 2020, **142**, 4807–4819.

69 W. Lv, S. Wang, P. Wang, Y. Liu, Z. Huang, J. Li, M. Dong, J. Wang and W. Fan, *J. Catal.*, 2021, **393**, 190–201.

70 J. Zhang, Y. Shan, L. Zhang, J. Du, H. He, S. Han, C. Lei, S. Wang, W. Fan, Z. Feng, X. Liu, X. Meng and F.-S. Xiao, *Appl. Catal., B*, 2020, **277**, 119193.

71 E. M. Flanigen and R. L. Patton, *US Pat.*, 4073865, 1978.

72 M. A. Camblor, L. A. Villaescusa and M. J. Díaz-Cabañas, *Top. Catal.*, 1999, **9**, 59–76.

73 M. Moliner, C. Martínez and A. Corma, *Angew. Chem., Int. Ed.*, 2015, **54**, 3560–3579.

74 D. Jo, G. T. Park, J. Shin and S. B. Hong, *Angew. Chem., Int. Ed.*, 2018, **57**, 2199–2203.

75 D. Jo and S. B. Hong, *Angew. Chem., Int. Ed.*, 2019, **58**, 13845–13848.

76 D. Jo, J. Zhao, J. Cho, J. H. Lee, Y. Liu, C. J. Liu, X. Zou and S. B. Hong, *Angew. Chem., Int. Ed.*, 2020, **59**, 17691–17696.

77 J. Bae and S. B. Hong, *Chem. Commun.*, 2018, **54**, 10997–11000.

78 J. Bae and S. B. Hong, *Microporous Mesoporous Mater.*, 2021, **327**, 111422.

79 H. S. Jacobsen, P. Norby, H. Bildsøe and H. J. Jakobsen, *Zeolites*, 1989, **9**, 491–495.

80 X. Zhao, L. Wang, J. Li, S. Xu, W. Zhang, Y. Wei, X. Guo, P. Tian and Z. Liu, *Catal. Sci. Technol.*, 2017, **7**, 5882–5892.

81 J. Chen, T. Liang, J. Li, S. Wang, Z. Qin, P. Wang, L. Huang, W. Fan and J. Wang, *ACS Catal.*, 2016, **6**, 2299–2313.

82 Y. Li, W. Guo, W. Fan, S. Yuan, J. Li, J. Wang, H. Jiao and T. Tatsumi, *J. Mol. Catal. A: Chem.*, 2011, **338**, 24–32.

83 C. Li, A. Vidal-Moya, P. J. Miguel, J. Dedecek, M. Boronat and A. Corma, *ACS Catal.*, 2018, **8**, 7688–7697.

84 S. Wang, S. Li, L. Zhang, Z. Qin, M. Dong, J. Li, J. Wang and W. Fan, *Catal. Sci. Technol.*, 2017, **7**, 4766–4779.

85 S. Wang, P. Wang, Z. Qin, Y. Chen, M. Dong, J. Li, K. Zhang, P. Liu, J. Wang and W. Fan, *ACS Catal.*, 2018, **8**, 5485–5505.

86 Y. Xue, J. Li, P. Wang, X. Cui, H. Zheng, Y. Niu, M. Dong, Z. Qin, J. Wang and W. Fan, *Appl. Catal., B*, 2021, **280**, 119391.

87 L. Li, Y. Chen, S. Xu, J. Li, M. Dong, Z. Liu, H. Jiao, J. Wang and W. Fan, *J. Catal.*, 2016, **344**, 242–251.

88 J. Jiang, J. Yu and A. Corma, *Angew. Chem., Int. Ed.*, 2010, **49**, 3120–3145.

89 S. B. Hong, S.-H. Lee, C.-H. Shin, A. J. Woo, L. J. Alvarez, C. M. Zicovich-Wilson and M. A. Camblor, *J. Am. Chem. Soc.*, 2004, **126**, 13742–13751.

90 J. Shin, N. H. Ahn, M. A. Camblor, S. J. Cho and S. B. Hong, *Angew. Chem., Int. Ed.*, 2014, **53**, 8949–8952.

91 J. Grand, H. Awala and S. Mintova, *CrystEngComm*, 2016, **18**, 650–664.

92 V. Pashkova, P. Klein, J. Dedecek, V. Tokarová and B. Wichterlová, *Microporous Mesoporous Mater.*, 2015, **202**, 138–146.

93 J. Dedecek, V. Balgová, V. Pashkova, P. Klein and B. Wichterlová, *Chem. Mater.*, 2012, **24**, 3231–3239.

94 Y. Joichi, D. Shimono, N. Tsunoji, Y. Takamitsu, M. Sadakane and T. Sano, *Cryst. Growth Des.*, 2018, **18**, 5652–5662.

95 N. Tsunoji, D. Shimono, K. Tsuchiya, M. Sadakane and T. Sano, *Chem. Mater.*, 2020, **32**, 60–74.

96 K. Yamamoto, S. E. B. Garcia, F. Saito and A. Muramatsu, *Chem. Lett.*, 2006, **35**, 570–571.

97 K. Yamamoto, S. E. B. García and A. Muramatsu, *Microporous Mesoporous Mater.*, 2007, **101**, 90–96.

98 S. E. B. Garcia, K. Yamamoto and A. Muramatsu, *J. Mater. Sci.*, 2008, **43**, 2367–2371.

99 K. Kanie, M. Sakaguchi, F. Muto, M. Horie, M. Nakaya, T. Yokoi and A. Muramatsu, *Sci. Technol. Adv. Mater.*, 2018, **19**, 545–553.

100 M. Yabushita, M. Yoshida, F. Muto, M. Horie, Y. Kunitake, T. Nishitoba, S. Maki, K. Kanie, T. Yokoi and A. Muramatsu, *Mol. Catal.*, 2019, **478**, 110579.

101 M. Yabushita, H. Kobayashi, A. Neya, M. Nakaya, S. Maki, M. Matsubara, K. Kanie and A. Muramatsu, *CrystEngComm*, 2020, **22**, 7556–7564.

102 M. Yabushita, H. Kobayashi, R. Osuga, M. Nakaya, M. Matsubara, S. Maki, K. Kanie and A. Muramatsu, *Ind. Eng. Chem. Res.*, 2021, **60**, 2079–2088.

103 M. Yabushita, Y. Imanishi, T. Xiao, R. Osuga, T. Nishitoba, S. Maki, K. Kanie, W. Cao, T. Yokoi and A. Muramatsu, *Chem. Commun.*, 2021, **57**, 13301–13304.

104 A. Deneyer, Q. Ke, J. Devos and M. Dusselier, *Chem. Mater.*, 2020, **32**, 4884–4919.

105 R. Jain, A. J. Mallette and J. D. Rimer, *J. Am. Chem. Soc.*, 2021, **143**, 21446–21460.

106 R. M. Barrer, L. Hinds and E. A. White, *J. Chem. Soc.*, 1953, 1466–1475.

107 M. Itakura, T. Inoue, A. Takahashi, T. Fujitani, Y. Oumi and T. Sano, *Chem. Lett.*, 2008, **37**, 908–909.

108 M. Itakura, I. Goto, A. Takahashi, T. Fujitani, Y. Ide, M. Sadakane and T. Sano, *Microporous Mesoporous Mater.*, 2011, **144**, 91–96.

109 L. Van Tendeloo, E. Gobechiya, E. Breynaert, J. A. Martens and C. E. A. Kirschhock, *Chem. Commun.*, 2013, **49**, 11737–11739.

110 Y. Ji, M. A. Deimund, Y. Bhawe and M. E. Davis, *ACS Catal.*, 2015, **5**, 4456–4465.

111 T. Takata, N. Tsunoji, Y. Takamitsu, M. Sadakane and T. Sano, *Microporous Mesoporous Mater.*, 2016, **225**, 524–533.

112 N. Nakazawa, T. Ikeda, N. Hiyoshi, Y. Yoshida, Q. Han, S. Inagaki and Y. Kubota, *J. Am. Chem. Soc.*, 2017, **139**, 7989–7997.

113 Q. Liu, Y. Yoshida, N. Nakazawa, S. Inagaki and Y. Kubota, *Materials*, 2020, **13**, 2030.

114 H. Lee, W. Choi, H. J. Choi and S. B. Hong, *ACS Mater. Lett.*, 2020, **2**, 981–985.

115 T. Nishitoba, N. Yoshida, J. N. Kondo and T. Yokoi, *Ind. Eng. Chem. Res.*, 2018, **57**, 3914–3922.

116 K. Muraoka, Y. Sada, A. Shimojima, W. Chaikittisilp and T. Okubo, *Chem. Sci.*, 2019, **10**, 8533–8540.

117 J. Devos, S. Robijns, C. Van Goethem, I. Khalil and M. Dusselier, *Chem. Mater.*, 2021, **33**, 2516–2531.

118 E. Dempsey, G. Kühl and D. H. Olson, *J. Phys. Chem.*, 1969, **73**, 387–390.

119 D. Suhendar, Buchari, R. R. Mukti and Ismunandar, *IOP Conf. Ser.: Mater. Sci. Eng.*, 2018, **349**, 012016.

120 W. Qin, R. Jain, F. C. Robles Hernández and J. D. Rimer, *Chem. – Eur. J.*, 2019, **25**, 5893–5898.

121 D. Schwalbe-Koda, Z. Jensen, E. Olivetti and R. Gómez-Bombarelli, *Nat. Mater.*, 2019, **18**, 1177–1181.

122 R. Jain and J. D. Rimer, *Microporous Mesoporous Mater.*, 2020, **300**, 110174.

123 J. Devos, M. A. Shah and M. Dusselier, *RSC Adv.*, 2021, **11**, 26188–26210.

124 T. Xiao, M. Yabushita, T. Nishitoba, R. Osuga, M. Yoshida, M. Matsubara, S. Maki, K. Kanie, T. Yokoi, W. Cao and A. Muramatsu, *ACS Omega*, 2021, **6**, 5176–5182.

125 N. Garg and J. Skibsted, *J. Am. Ceram. Soc.*, 2019, **102**, 7720–7734.

126 Z. Liu, A. Chokkalingam, S. Miyagi, M. Yoshioka, T. Ishikawa, H. Yamada, K. Ohara, N. Tsunoji, Y. Naraki, T. Sano, T. Okubo and T. Wakihara, *Phys. Chem. Chem. Phys.*, 2022, **24**, 4136–4146.

127 P. Wagner, Y. Nakagawa, G. S. Lee, M. E. Davis, S. Elomari, R. C. Medrud and S. I. Zones, *J. Am. Chem. Soc.*, 2000, **122**, 263–273.

128 M. Dusselier, J. E. Schmidt, R. Moulton, B. Haymore, M. Hellums and M. E. Davis, *Chem. Mater.*, 2015, **27**, 2695–2702.

129 R. Li, N. Linares, J. G. Sutjianto, A. Chawla, J. Garcia-Martinez and J. D. Rimer, *Angew. Chem., Int. Ed.*, 2018, **57**, 11283–11288.

130 D. Parmar, Z. Niu, Y. Liang, H. Dai and J. D. Rimer, *Faraday Discuss.*, 2022, **235**, 322–342.

131 M. J. Mendoza-Castro, E. De Oliveira-Jardim, N.-T. Ramírez-Marquez, C.-A. Trujillo, N. Linares and J. García-Martínez, *J. Am. Chem. Soc.*, 2022, **144**, 5163–5171.